ELSEVIER

Journal of Alloys and Compounds 365 (2004) 8–14

Journal of ALLOYS AND COMPOUNDS

www.elsevier.com/locate/jallcom

Structural, optical and photoelectrical properties of vacuum evaporated $Cd_{0.3}Sn_{0.7}Se$ thin films

D. Pathinettam Padiyan [a,*], A. Marikani [b], K.R. Murali [c]

[a] *Department of Physics, Manonmaniam Sundaranar University, Tirunelveli 627-012, India*
[b] *Mepco Schlenk Engineering College, Virudhunagar-Dt. 626-005, India*
[c] *Central Electrochemical Research Institute, Karaikudi 630-006, India*

Received 12 March 2003; received in revised form 2 June 2003; accepted 2 June 2003

Abstract

Polycrystalline $Cd_{0.3}Sn_{0.7}Se$ thin films were prepared in four different thicknesses on glass substrates by vacuum evaporation technique at room temperature and subsequently annealed in air at 300 °C for 2 h. They possess a single crystalline phase. The structural, electrical, optical and photoelectrical properties of these films were studied. The lattice parameters of the synthesized compound and the optical band gaps of thin films were estimated and the results are discussed in detail.

Keywords: Semiconductors; Thin films; Vacuum deposition; Electrical transport; Photoconductivity

1. Introduction

Metal chalcogenides offer a wide range of optical band gaps suitable for various optical and optoelectronic applications. Cadmium selenide has been investigated for many years for its potential applications in electrography, photovoltaic cells, thin film transistors and lasers [1–4]. Thin films of tin selenide have numerous applications as solar cell memory, switching devices and holographic recording system [5–8]. CdSe and SnSe have been studied in the form of both thin films and single crystals [9–12]. CdSe is a narrow band semiconductor and its optical band gap is 1.74 eV [13], whereas SnSe has a band gap energy of 0.9 eV [14]. Since there is no study has been reported in the literature for $Cd_xSn_{1-x}Se$ solid solution either in the form of thin films or single crystals, we made an attempt to synthesize and characterize $Cd_{0.3}Sn_{0.7}Se$ thin films. In this paper, we report the variation of the band gap with thickness and the photoconducting properties of these vacuum evaporated thin films.

2. Experimental

$Cd_{0.3}Sn_{0.7}Se$ material was synthesized in a quartz ampoule by taking cadmium metal, tin and selenium powders (Aldrich, 99.99%) in stoichiometric ratio. The ampoule was evacuated to a pressure of 10^{-3} Pa, sealed and it was kept at the uniform temperature zone of the furnace. The temperature was gradually increased up to 900 °C and maintained at this temperature for a period of 10 h. During this period, the ampoule was rotated to ensure complete mixing and then it was slowly cooled to room temperature. The synthesized compound was analyzed by the X-ray diffraction (XRD) technique for its homogeneity and crystalline nature.

The thin films of these materials were deposited on glass substrates by vacuum evaporation. The substrates were thoroughly cleaned in a detergent solution and then in chromic acid and finally, cleaned using trichloroethylene. Double distilled water was used throughout the different stages of cleaning. The thin films were prepared in a vacuum coating unit (Hind Hivac Coating Unit, model 12-A4) at a pressure of 10^{-4} Pa using the synthesized powder material. The synthesized powder material was taken in a molybdenum boat. The temperature of the molybdenum boat was raised to 900 °C. The glass substrates placed at about 15 cm above the source were not heated except through any heat transfer

* Corresponding author. Fax: +91-462-232-2973.
E-mail address: dppadiyan@rediffmail.com (D. Pathinettam Padiyan).

0925-8388/$ – see front matter © 2003 Elsevier B.V. All rights reserved.
doi:10.1016/S0925-8388(03)00648-0

from this heated source. The rate of coating was maintained at 2 nm s^{-1}. The films obtained in the above conditions were reproducible and possess a metallic luster. A quartz crystal film thickness monitor was used. The thicknesses of the films were measured by forming interference fringes [15]. Thin films were prepared at four different thicknesses namely 0.225 μm, 0.276 μm, 0.300 μm and 0.683 μm at room temperature.

The X-ray diffraction patterns for the synthesized powder sample and thin films were recorded in a Jeol JDX 8030 X-ray diffractometer using Cu Kα radiation. The composition of the powder sample was determined using the atomic absorption spectroscopy technique. The optical transmission spectra were recorded using a UV–Vis–NIR spectrophotometer (Hitachi V-3400) in the wavelength region 400 to 2000 nm for all the samples having different thicknesses prepared at room temperature (303 K). The composition and elemental analyses of the as-prepared thin film were carried out using X-ray photoelectron spectroscopy. The X-ray photoelectron spectra were recorded with an Escalab MK II spectrometer (VG Scientific Ltd, UK) using Mg Kα radiation of energy 1253.6 eV. The electrical conductivity measurements were studied by the van der Pauw technique from 302 K to 493 K. For electrical measurements, the ohmic contacts were made using high purity silver paste (Eltecks Corporation, Bangalore) and gold electrodes. The photoconductivity measurements were made using a halogen (100 W) lamp fed by a constant voltage supply.

3. Results and discussions

3.1. X-ray diffraction

3.1.1. Synthesized compound

Fig. 1 shows the powder X-ray diffraction pattern of the synthesized compound. The XRD data of the powder sample was indexed using the Hull and Davey chart [16]

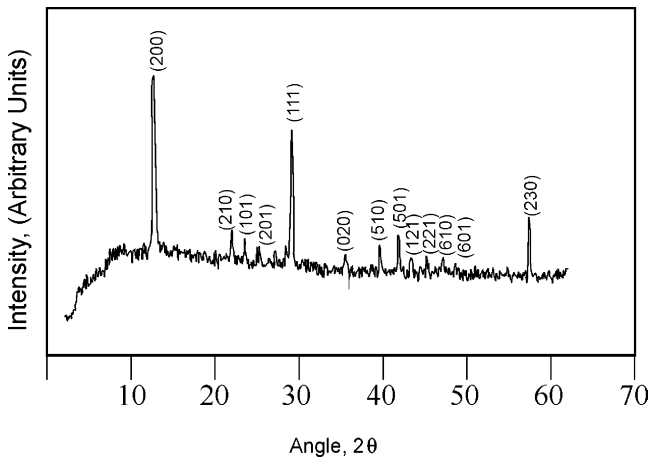

Fig. 1. X-ray diffraction pattern of synthesized $Cd_{0.3}Sn_{0.7}Se$ powder material indexed with the help of the powder indexing program, DICVOL91.

Table 1
XRD data for $Cd_{0.3}Sn_{0.7}Se$ synthesized powder material indexed using the program DICVOL91

Sl. no.	*hkl*	2θ (degree)	*d* (Å) observed	*d* (Å) calculated	$I/I_o \times 100$
1.	(200)	14.4	6.146	6.055	100
2.	(210)	23.8	3.736	3.734	44
3.	(101)	25.3	3.517	3.617	41
4.	(201)	27.2	3.276	3.216	40
5.	(111)	31.0	2.882	2.879	63
6.	(020)	37.7	2.384	2.376	36
7.	(510)	42.0	2.149	2.158	36
8.	(501)	44.3	2.043	2.041	39
9.	(121)	45.8	1.980	1.986	33
10.	(221)	47.7	1.905	1.910	33
11.	(610)	49.7	1.833	1.858	34
12.	(601)	51.2	1.783	1.782	31
13.	(230)	60.4	1.531	1.532	38

and a powder XRD indexing program, DICVOL91 [17,18]. Table 1 lists the characteristic lines, *hkl* values, 2θ of the compound and its interplanar spacings *d*. The cell parameters were refined with the help of the software known as UNITCELL [19]. It is found that the $Cd_{0.3}Sn_{0.7}Se$ powder material crystallizes in the orthorhombic crystal system with $a = (12.11 \pm 0.02)$ Å, $b = (4.751 \pm 0.007)$ Å, and $c = (3.79 \pm 0.02)$ Å [20]. The composition analysis of the synthesized powder material was carried out using atomic absorption spectrophotometry. The composition of the synthesized powder material was found to be selenium deficient with cadmium 15.4%, tin 35.9% and selenium 48.7%.

3.1.2. Thin films

The X-ray diffraction patterns recorded for the as-prepared thin films did not show any peak, indicating that the films are of poor crystallinity. However, the thin films of thicknesses 0.225 μm and 0.276 μm, 0.3 μm and 0.683 μm annealed at 300 °C for 2 h in air give rise to X-ray peaks, as shown in Fig. 2. Thin films of thicknesses 0.225 μm and 0.276 μm show one X-ray peak each, whereas two X-ray peaks are noticed in 0.3 μm and 0.683 μm thick films. These X-ray peaks are indexed and the measured *d*-values for (200) and (210) are in agreement with the synthesized powder data and given in Table 2. The (200) X-ray peak observed in these films (Fig. 2) reveals that annealed films have a preferential orientation and their crystallites have their (200) axis perpendicular to the film plane. However for the thin film of thickness 0.683 μm (Fig. 2d) preferential orientation along (210) is observed. A similar preferential orientation is reported in semiconductor thin films by various workers [21–24]. The broad peak appearing in the low angle is due to the (amorphous) glass substrate itself.

3.2. XPS analysis

The XPS spectra of the as-deposited thin film of thickness 0.3 μm are given in Fig. 3. Presence of chemisorbed

Table 2
XRD data for $Cd_{0.3}Sn_{0.7}Se$ thin films annealed at 300 °C for various thicknesses

Sl. no.	Thickness (μm)	2θ (degree)	Intensity, *I*	*d* (Å) measured (powder sample)	*d* (Å) (calculated using refined *a*,*b*,*c* values)	*hkl*
1.	0.225	14.6	79	6.062	6.146	(200)
2.	0.276	14.3	711	6.189	6.146	(200)
3.	0.300	14.6	120	6.062	6.146	(200)
4.	0.300	24.2	91	3.675	3.736	(210)
5.	0.683	14.6	175	6.062	6.146	(200)
6.	0.683	23.6	178	3.767	3.736	(210)

oxygen is observed in the surface layer for the film stored in the presence of atmospheric oxygen. On sputtering a thin layer of the film, it is found that the concentration of oxygen decreases. This is due to the well known fact of oxygen chemisorption mechanism in metal chalcogenide films. The measured positions of the XPS peaks are given in Table 3. The binding energy values of the XPS peaks are calibrated with respect to carbon 1s line of the hydrocarbon contamination of spectrometer chamber as an internal standard of 284.0 eV. The shift in the measured peak positions of Cd and Sn to the higher energy side compared to their standard values of 410.5 eV (Cd($3d_{3/2}$)), 484.8 eV (Sn($3d_{5/2}$)) and 493.3 (Sn($3d_{3/2}$)) is due to electrostatic charging [25]. Selenium $3P_{3/2}$ and $3P_{1/2}$ are observed at 158.1 eV and 165.1 eV with a separation energy of 7.0 eV as shown in Fig. 3c. A satellite feature have been noticed at 150 eV and is due to the charge transfer transition.

The atomic concentration of elements in these thin films are calculated using the area and the intensity ratio of the XPS peaks, showing that the film is selenium rich and

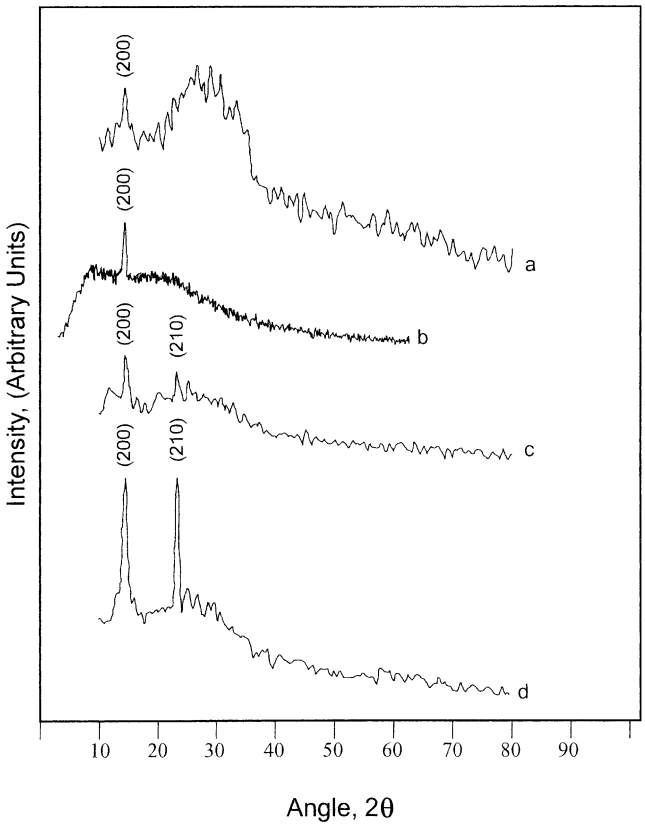

Fig. 2. XRD patterns of thin films annealed at 300 °C and of thicknesses (a) 0.225 μm, (b) 0.276 μm, (c) 0.300 μm and (d) 0.683 μm.

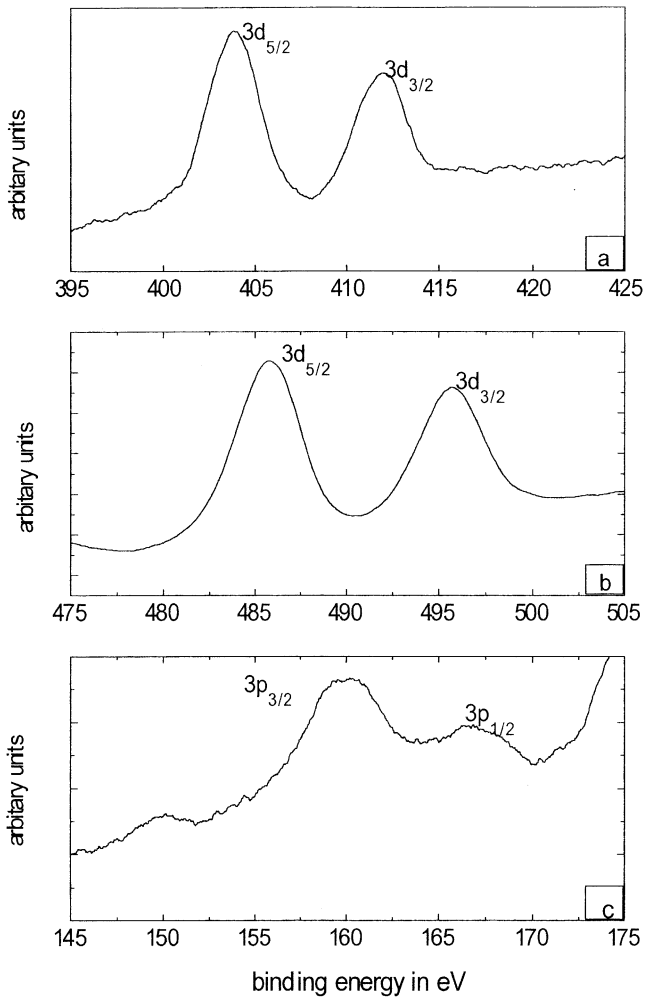

Fig. 3. XPS peaks of (a) Cd, (b) Sn and (c) Se measured for as prepared $Cd_{0.3}Sn_{0.7}Se$ thin film of thickness 0.3 μm.

Table 3
Binding energy of various XPS peaks measured for as prepared $Cd_{0.3}Sn_{0.7}Se$ thin film of thickness 0.3 μm

Substance	Measured peak positions (eV)	Standard values (eV)
$Cd(3d_{5/2})$	403.8	403.7
$Cd(3d_{3/2})$	411.9	410.5
$Sn(3d_{5/2})$	485.7	484.8
$Sn(3d_{3/2})$	495.6	493.3
$Se(3p_{3/2})$	158.1	161.9
$Se(3p_{1/2})$	165.1	168.2

cadmium deficient and found to have cadmium 13.2%, tin 34.0% and selenium 52.8%. The selenium rich in $Cd_{0.3}Sn_{0.7}Se$ thin film is due to the higher deposition rate and source temperature. Similar change of film composition in CdSe from Cd rich to Se rich due to the increase in the deposition rate and source temperature has been reported by Chan and Hill [26]. The change of Cd rich to Se rich is also expected from the consideration of the vapor pressure curves for Cd and Se [27]. These curves show that the vapor pressure becomes increasingly rich in selenium as the source temperature increases.

3.3. Optical properties

The films are found to have a light brown color at 0.225 μm and change to dark brown color as the thickness increases to 0.683 μm. The optical absorption coefficient α is determined using the relation

$$\alpha = \frac{2.303}{t}\log_{10}\left(\frac{1}{T}\right) \quad (1)$$

where t is the thickness of the film and T is the transmittance. The relation between the absorption coefficient and the photon energy $h\nu$ is [28]:

$$\alpha h\nu = [h\nu - E_g \pm E_p]^n \quad (2)$$

where E_p is the phonon energy and E_g is the energy gap. For direct transition ($E_p = 0$), n is equal to 0.5 and 1.5 for allowed and forbidden transitions respectively. For indirect transitions, n is equal to 2 for allowed transitions and 3 for forbidden transitions. In the present work, the value of α is found to be in the order of 10^6 m^{-1}, and since the absorption coefficient is measured at room temperature, the presence of exciton bands is not likely to be possible. So, the indirect band gap is not probable [29,30] and the band gap is only due to an allowed direct transition from the top of the valence band to the bottom of the conduction band at the center of the Brillouin zone.

A plot of $(\alpha h\nu)^2$ as a function of $h\nu$ for the as-deposited thin films for four different thicknesses is shown in Fig. 4. They are linear in the strong absorption near the fundamental absorption edge, thus supporting the interpretation of the direct band gap for all thin films. The band gap energy values determined for the thin films of thicknesses 0.225 μm, 0.276 μm, 0.300 μm and 0.683 μm are 2.17 eV, 2.13 eV, 2.11 eV and 2.07 eV, respectively, and are shown in Table 4. It is noted that the band gap value decreases with increasing film thickness. Such a variation in band gap value with the increase in film thickness has been reported by Shaalan and Müller [31] for their thermally evaporated CdSe thin films and also by Pal et al. [32] for their vacuum evaporated polycrystalline CdSe samples.

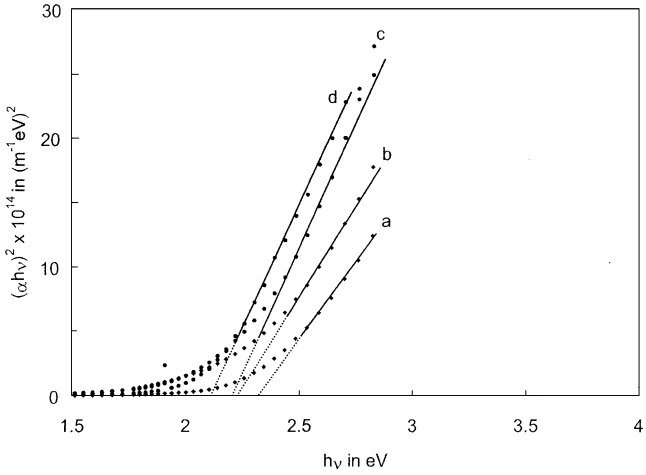

Fig. 4. A plot of $(\alpha h\nu)^2$ versus $h\nu$ for the as-prepared thin films of thicknesses (a) 0.225 μm, (b) 0.276 μm, (c) 0.300 μm and (d) 0.683 μm.

The decrease in band gap with the increase in thickness of thin films is attributed to the smaller grain size of the material [33]. This variation can be explained in terms of quantum size effect and of high dislocation density [14,34]. It is well known that the shift of optical band gap to higher value compared to its single crystal value is attributed to very small grain size of 3–10 nm and the resulting quantum confinement of electronic states in thin films. Since there is no reported band gap value for a $Cd_{0.3}Sn_{0.7}Se$ single crystal, it is not possible to compare the band gap values with the bulk samples.

In semiconductor and semimetal thin films, the quantum size effect appears when the thickness of the films are comparable with the mean free path and the effective de-Broglie wavelength of the carriers. The transverse component of the quasi-momentum of the carrier is quantized due to the finite size of the thickness. Therefore, the transverse components of the electron states assume quasi-discrete energy values in a thin film. Due to this quantization, the bottom of the con-

Table 4
Variation of optical band gaps with thickness for $Cd_{0.3}Sn_{0.7}Se$ thin films

Sl. no.	Thickness (μm)	Band gap (eV)	ΔE (eV)
1.	0.225	2.170	0.226
2.	0.276	2.130	0.150
3.	0.300	2.110	0.110
4.	0.683	2.070	0.030

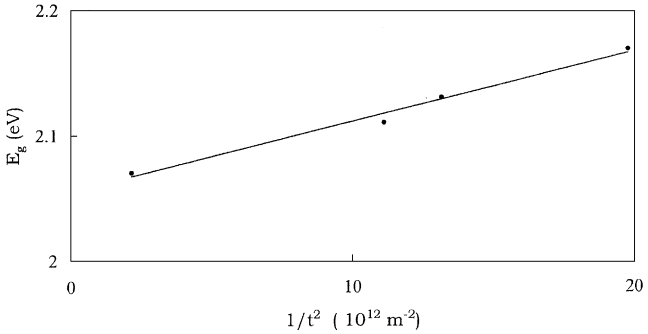

Fig. 5. A plot between E_g and $1/t^2$ for $Cd_{0.3}Sn_{0.7}Se$ thin films.

duction band and the top of the valence band are separated by an additional amount ΔE, given by [14]:

$$\Delta E \approx \frac{h^2}{8m * t^2} \quad (3)$$

where t is the thickness of the film and $m*$ is the effective mass of the carrier. The variation of the energy gap for as-deposited thin films with $1/t^2$, where t is the thickness of the film, is shown in Fig. 5 and is found to be linear. The decrease in the band gap energy with the increase of film thickness may be attributed to the quantization effect. In Fig. 5, the intercept at $x = 0$ yields the E_o value of 2.055 eV and hence the additional contribution of ΔE are calculated and given in Table 4.

3.4. Electrical properties

The electrical conductivity for as-deposited $Cd_{0.3}Sn_{0.7}Se$ thin films having thicknesses 0.225 μm, 0.276 μm, 0.300 μm and 0.683 μm measured in the temperature region 302 K to 493 K is shown in Fig. 6. It is seen that there are two distinct linear regions for the films of 0.225 μm, 0.276 μm and 0.300 μm thicknesses and one linear region for the film of thickness 0.683 μm. The plot reveals that these distinct regions possess Arrhenius behavior. The activation energy

Table 5
Activation energies ΔE_1 and ΔE_2 obtained for different thicknesses of $Cd_{0.3}Sn_{0.7}Se$ thin films

Sl. no.	Thickness (μm)	σ at 313 K (Sm^{-1})	Linear region	Activation energy (eV)
1.	0.225	4.318×10^{-3}	I 353 to 393 K II 403 to 523 K	0.226 0.733
2.	0.276	1.376×10^{-4}	I 353 to 403 K II 403 to 523 K	0.295 0.626
3.	0.300	2.228×10^{-4}	I 353 to 413 K II 413 to 493 K	0.424 0.850
4.	0.683	8.830×10^{-5}	I 343 to 463 K	0.862

calculated for these four samples are listed in Table 5. In the first linear region, the increase in electrical conductivity with temperature is due to the intrinsic nature of the film. In this temperature region, there is no adequate number of charge carriers due to its intrinsic defects and the mobility of the charge carriers is low. Above these temperatures, the conductivity increases rapidly with the increase of temperature. This behavior is due to the creation of more charge carriers with the increase of temperature. The low mobility of the charge carriers is easily compensated by the creation of a large number of charge carriers and there is an increase in the conductivity of the specimen [30]. Hence, the activation energy in region II is greater than region I in these thin films. From Fig. 6, it is also observed that the electrical resistivity increases with the increase of thickness.

3.5. Photoconductivity

3.5.1. Steady-state photoconductivity

The dark current and the photocurrents recorded for as-deposited $Cd_{0.3}Sn_{0.7}Se$ thin films having thickness 0.276 μm for different light intensity levels (600 lux, 1800 lux and 3000 lux) at room temperature are shown in Fig. 7. The photocurrent on illumination is obtained by subtracting the dark current from the total current measured. The

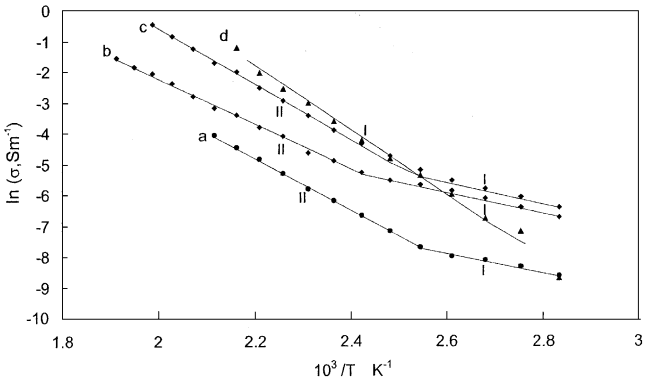

Fig. 6. A plot of ln σ against $10^3/T$ from 302 K to 493 K for as-deposited $Cd_{0.3}Sn_{0.7}Se$ thin films of thicknesses (a) 0.225 μm, (b) 0.276 μm, (c) 0.300 μm and (d) 0.683 μm.

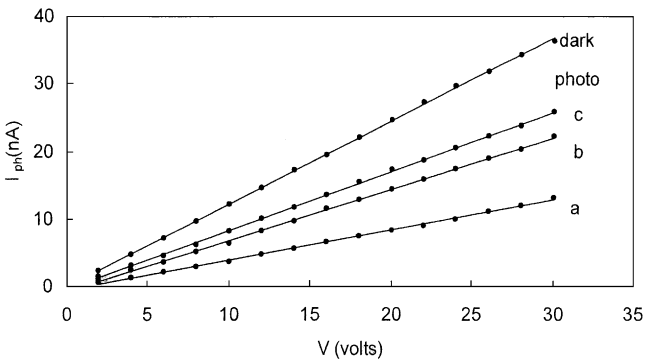

Fig. 7. The steady-state photoconductivity of as-deposited $Cd_{0.3}Sn_{0.7}Se$ thin film of thickness 0.276 μm illuminated at (a) 600 lux, (b) 1800 lux and (c) 3000 lux.

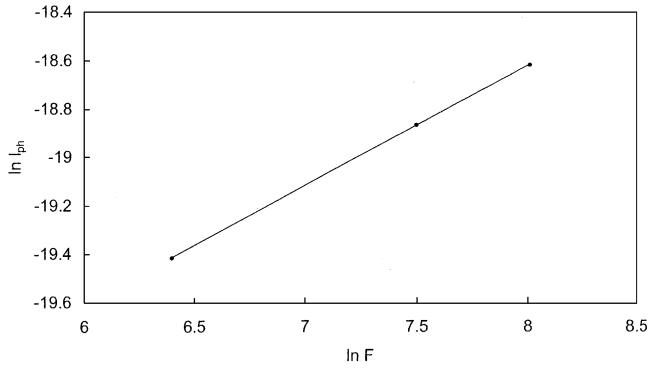

Fig. 8. A plot of ln I_{ph} versus ln F for as-deposited $Cd_{0.3}Sn_{0.7}Se$ thin film of thickness 0.276 μm.

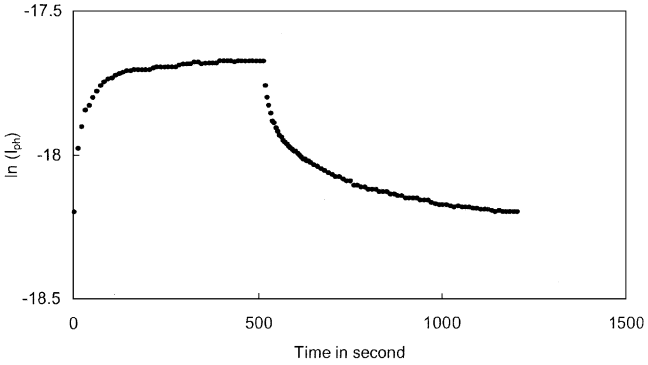

Fig. 9. Photodecay of as-deposited $Cd_{0.3}Sn_{0.7}Se$ thin film of thickness 0.276 μm.

dark conductivity and the total conductivity obtained for an applied voltage of 10 V for the light intensity of 3000 lux are 3.09×10^{-6} Sm^{-1} and 2.07×10^{-6} Sm^{-1}, respectively. The experimental results show that the photoconductivity increases with the photo illumination and it is due to the generation of free charge carriers. The slope of the current–voltage characteristics increases with increase in the illumination level F.

A plot is drawn between the photocurrent and illumination level on a logarithmic scale for the as-deposited thin films of thickness 0.276 μm and is shown in Fig. 8. The straight line observed indicates that there exists a relationship between the photocurrent and illumination level. The photocurrent follows a power law of the form:

$$I_{ph} \propto F^{\gamma} \tag{4}$$

where γ is a constant and its value determines the recombination process [35]. For bimolecular recombination process, the value of γ is equal to 0.5 and for monomolecular recombination process, the exponent γ is equal to 1. If the value of γ lies in between 0.5 and 1, it represents the continuous distribution of localized states. In the present case, the value of γ is found to be 0.495 and it is close to 0.5 revealing that the bimolecular recombination mechanism is followed in these films. A similar bimolecular recombination mechanism behavior has been reported by Mann et al. [36] for their a-$Sb_{15}Ge_{10}Se_{75}$ thin films.

3.5.2. Transient photoconductivity

The transient photoconductivity measurements are carried out by exposing the as-deposited thin films ($t = 0.276$ μm) to light and simultaneously the photocurrent is recorded. Then the light is turned off and the current decay is followed. Fig. 9 shows the photo decay curve obtained by applying a potential difference of 10 V at room temperature for the as-deposited film illuminated by light intensity of 3000 lux.

The long photocurrent rise time and slow decay process observed in these thin films is due to the presence of the deep localized gap states in these materials. The slow decay process can be explained using the concept of differential life time τ_d [37] and

$$\tau_d = -\left[\frac{1}{I'_{ph}}\frac{dI_{ph}}{dt}\right]^{-1} \tag{5}$$

where I'_{ph} is the maximum photocurrent at $t = 0$.

The decay time observed for the $Cd_{0.3}Sn_{0.7}Se$ vacuum evaporated thin films is found to be time dependent. In the case of non-exponential decay τ_d is not a constant and increases with time. At $t = 0$, τ_d gives the value of the carrier lifetime. In order to find the nature of decay τ_d is plotted against time t on a logarithmic scale for the as-deposited film of thickness 0.276 μm and shown in Fig. 10. It shows that there is a linear relationship between ln τ_d and ln t, indicating that the decay is time dependent. This straight line obeys the power law of the form t^n, with

$$n = \frac{d(\ln\tau_d)}{d(\ln t)} \tag{6}$$

Moreover, the value of n is found to be 1.042.

The photosensitivity of the film is determined using the relation,

$$S = \frac{\sigma_{ph}}{\sigma_d} \tag{7}$$

where σ_{ph} is the electrical conductivity of the sample when illuminated by light and σ_d is the dark conductivity of the

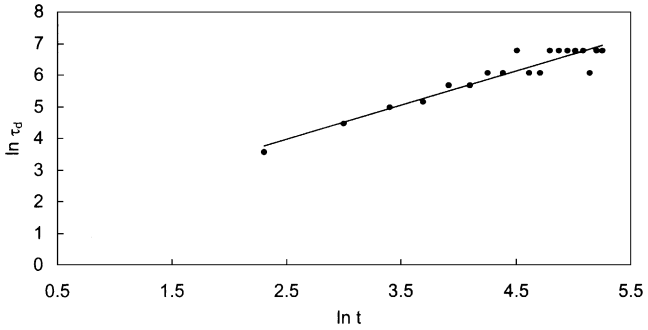

Fig. 10. A plot of ln τ_d versus ln t for as-deposited $Cd_{0.3}Sn_{0.7}Se$ thin film of thickness 0.276 μm.

sample. The photosensitivity of the films for an applied potential difference of 10 V is 0.30, 0.52 and 0.67 for 600 lux, 1800 lux and 3000 lux, respectively. This indicates that the photosensitivity increases with increase in the intensity of the light and the material is found to be photosensitive.

4. Conclusion

Polycrystalline $Cd_{0.3}Sn_{0.7}Se$ materials have been synthesized by the melt technique. The XRD pattern showed that the synthesized powder material crystallizes in orthorhombic crystal structure with lattice constants $a = (12.11 \pm 0.02)$ Å, $b = (4.751 \pm 0.007)$ Å, and $c = (3.79 \pm 0.02)$ Å. Thin films of these materials have been prepared for four different thicknesses using a vacuum evaporation technique. The structural, electrical, optical and photoconducting properties are studied. X-ray photoelectron spectroscopic analysis indicates that the vacuum evaporated films are selenium rich and cadmium deficient. The films on storage in air adsorb oxygen, which is a common feature of metal chalcogenide films. The optical studies reveal that these films has a direct band gap and the band gap energy varies from 2.17 to 2.07 eV with thickness. The variation of band gap with thickness is due to the quantization of the quasi-momentum of the charge carriers and is explained using the quantum size effect concept. The photoconductivity studies showed that the existence of the deep localized states and the thin films are found to be photosensitive.

Acknowledgements

The authors thank the Department of Science and Technology, Government of India for their financial support. We thank the Regional Sophisticated Instrumentation Centre at Indian Institute of Technology, Chennai for XPS spectra measurement. One of the authors (AM) thanks the Principal and the Management of Mepco Schlenk Engineering College, Sivakasi for their constant encouragement of this work.

References

[1] D. Samanta, B. Samanta, A.K. Chaudhuri, S. Ghorai, U. Pal, Semicond. Sci. Technol. 11 (1996) 548.
[2] S. Eriksson, T. Gruszecki, P. Carlsson, B. Holmström, Thin Solid Films 269 (1995) 14.
[3] S.M. Boudreau, R.D. Rauh, R.A. Boudreau, J. Chem. Educ. 60 (1983) 498.
[4] M.A. Russak, J. Reichman, H. Witzke, S.K. Deb, S.N. Sen, J. Electrochem. Soc. 127 (1980) 725.
[5] C.R. Baxter, W.D. McLennan, J. Vac. Sci. Technol. 12 (1975) 110.
[6] A. Bennouna, P.Y. Tessier, M. Priol, Q. Dang Tran, S. Robin, Phys. Status Solidi (b) 117 (1983) 51.
[7] M. Rodat, Acta Electronic. 18 (1975) 345.
[8] R.M. Dongwoo Chu, R.W.B. Walser, T.H. Courtney, Appl. Phys. Lett. 24 (1974) 479.
[9] A. Agarwal, P.D. Patel, D. Lakshminarayana, J. Cryst. Growth 142 (1994) 344.
[10] H.S. Soliman, D.A. Abdel Hady, K.F. Abdel Rahman, S.B. Youssef, A.A. El-Shazly, Physica A 216 (1995) 77.
[11] S. Velumani, X. Mathew, P.J. Sebastian, S.K. Narayanadass, D. Mangalaraj, Solar Energy Mater. 76 (2003) 347.
[12] O.O. Adetunji, N. Roy, Y. Cui, G. Wright, J.-O. Ndap, A. Burger, J. Electron. Mater. 31 (2002) 795.
[13] D.R. Lide, H.P.R. Frederikse (Eds.), CRC Handbook of Chemistry and Physics, 75the Edition, CRC Press, USA, 1994, pp. 12–95.
[14] V.P. Bhatt, K. Gireesan, C.F. Desai, Cryst. Res. Technol. 24 (1989) 187.
[15] E.A. Corl, H. Wimpfheimer, Solid State Electron. 7 (1964) 755.
[16] B.D. Cullity, Elements of X-ray Diffraction, Addison-Wesley, Massachusetts, 1978 p. 324.
[17] D. Louër, M. Louër, J. Appl. Crystallogr. 5 (1972) 271.
[18] A. Boultif, D. Louër, J. Appl. Crystallogr. 24 (1991) 987.
[19] T.J.B. Holland, S.A.T. Redfern, Mineralog. Mag. 61 (1997) 65.
[20] D. Pathinettam Padiyan, A. Marikani, Cryst. Res. Technol. 37 (2002) 1241.
[21] D. Pathinettam Padiyan, A. Marikani, K.R. Murali, Cryst. Res. Technol. 35 (2000) 949.
[22] M.T.S. Nair, P.K. Nair, R.A. Zingaro, E.A. Meyers, J. Appl. Phys. 74 (1993) 1879.
[23] V.M. Garcia, P.J. George, M.T.S. Nair, P.K. Nair, J. Electrochem. Soc. 143 (1996) 2892.
[24] S. Shigetomi, M. Ohkubo, T. Ikari, Thin Solid Films 199 (1991) 215.
[25] C.D. Wagner, W.M. Riggs, L.E. Davis, T.F. Moulder, G.E. Muilenberg, Handbook of X-ray Photoelectron Spectroscopy, Perkin-Elmer, Norwalk, CT, 1978 p. 182.
[26] D.S.H. Chan, A.E. Hill, Thin Solid Films 38 (1976) 163.
[27] K.G. Gunther, in: J.C. Anderson (Ed.), The Use of Thin Films in Physical Investigations, Academic Press, London, 1966.
[28] D.T. Quan, Phys. Status Solidi (a) 86 (1984) 421.
[29] K.J. John, B. Pradeep, E. Mathai, J. Mater. Sci. 29 (1994) 1581.
[30] R.A. Smith, Semiconductors, 1st Edition, , Cambridge University Press, Cambridge, 1959 p. 116.
[31] M.S. Shaalan, R. Müller, Solar Cells 28 (1990) 185.
[32] U. Pal, D. Samanta, S. Ghorai, A.K. Chaudhuri, J. Appl. Phys. 74 (1993) 6368.
[33] V.M. Garcia, M.T.S. Nair, P.K. Nair, R.A. Zingaro, Semicond. Sci. Technol. 11 (1996) 427.
[34] V. Damodara Das, M.S. Jagadeesh, Mater. Res. Bull. 16 (1981) 1547.
[35] A. Rose, Concepts in Photoconductivity, Wiley-Interscience, New York, 1963 p. 64.
[36] A.S. Mann, A.K. Sharma, D.R. Goyal, J. Non-Cryst. Solids 104 (1998) 273.
[37] W. Fuhs, D. Meyer, Phys. Status Solidi (a) 24 (1974) 275.